Influence of crystals distribution on the photoluminescence properties of nanocrystalline silicon thin films

M. F. Cerqueira[1], M. Stepikhova[2], M. Losurdo[3], M.M. Giangregorio[3], E. Alves[4], T. Monteiro[5], M.J. Soares[5], C. Boemare[5]

[1] Departamento de Física, Universidade do Minho, Campus de Gualtar 4710-057 Braga, Portugal

[2] Institute for Physics of Microstructures RAS, 603600 Nizhnij Novgorod GSP-105, Russia

[3] Centro di Studio per la Chimica dei Plasmi, Dipartamento di Chimica Universita´ di Bari, Via Orabona n.4-70126 Bari, Italy

[4] Instituto Técnico Nuclear ITN, EN 10, 2686-953, Sacavém, Portugal

[5] Departamento de Física, Universidade de Aveiro, Campus de Santiago 3700 Aveiro, Portugal

Abstract

Nanocrystalline silicon thin films doped with erbium were produced by reactive magnetron RF sputtering. Their structural and chemical properties were studied by X-ray diffractometry at grazing incidence, micro-Raman, spectroscopic ellipsometry and Rutherford Backscattering Spectroscopy, respectively. Films with different crystalline fraction and crystallite size were deposited. Since the luminescence efficiency of Er-doped nc-Si films is strongly influenced by the microstructure and impurity content (i.e. H, O, Er), the photoluminescence characteristics are discussed in terms of the microstructure. The novelty of these films, if compared to usually investigated structures with the nanocrystals embedded in SiO2, is their relative high conductivity, which makes them attractive for device applications.

Keywords: Photoluminescence, Erbium, nanocrystalline silicon, ellipsometry

1. Introduction

Both, nanocrystalline silicon (nc-Si) and Er-doped silicon have been attracting enormous interest of researchers as promising candidates for the realization of Si-based visible and infrared light emitters [1]. Er-doped silicon takes special significance for optical communication systems due to the emission line at 1.54 μm. However, bulk crystalline c-Si:Er operating under forward bias still present unsolved problems like the strong temperature quenching of Er emission [2]. The situation may be considerably improved by incorporation of Er ions in nc-Si. This idea is based on the band-gap widening of nanometer size Si, which consequently has to result in a reducing of thermal quenching for Er luminescence.

Besides the studies in undoped samples, an intense research work has been devoted in the last years to nc-Si thin films intentionally doped with Er. Evidences have been reported that Er-doped nc-Si thin films have enhanced intra-ionic luminescence and reduced thermal quenching with respect to crystalline Si [3–6]. The reported data point to the acting of nc-Si confined excitons as efficient sensitizers for the rare earth luminescence. Also in this case, controversial results have been obtained both for the Er-related radiative lifetime and quenching mechanisms, as pointed by Ref. [7].

In this paper, we report on infrared PL properties of Er doped nc-Si thin films grown by RF co-sputtering. The electrical conductivity of such microcrystalline films is much higher than for a-Si [8].We will discuss the results on microstructure of samples with high, medium, low-crystallinity and of amorphous silicon and correlate the microstructure to photoluminescence (PL) properties.

2. Experimental

Erbium doped nanocrystalline silicon (nc-Si:Er) thin films were grown by RF reactive magnetron sputtering in an Ar/H_2 atmosphere on ordinary glass substrates under several different conditions using a procedure similar to that applied for the preparation of undoped mc-Si:H films [9], but adding small pieces of metallic erbium to the c-Si target.

Samples with different structural parameters, were obtained by varying the experimental parameters. In particular, a partially amorphous film (Er28) was obtained at low hydrogen dilution. Nanocrystalline samples were grown in a H_2 rich atmosphere, where the role of atomic hydrogen is to etch preferentially the amorphous phase and promote the amorphous-to-crystalline transition [10]. Growth conditions are presented in Table 1. The chemical composition (Table 2) was determined by Rutherford backscattering spectroscopy (RBS) and elastic recoil detection technique. For the structural characterisation, we used micro-Raman spectroscopy under excitation with 514.5 nm line of Ar_+ laser and X-ray diffractometry (XRD) in the grazing incidence geometry (incidence angle was fixed at 0.5^o). Spectroscopic ellipsometry (SE) was also used to analyse the film structure. Spectra were analysed using models based on the Bruggeman effective medium approximation, BEMA [11]. PL measurements in the infrared spectral region have been performed with a Brucker 66V Fourier-transform spectrometer.

Table 1: Growth conditions for Erbium doped nanocrystalline silicon thin films

Sample	Temperature (ºC)	RF power (W)	R_H
Er19	200	80	0.63
Er22	400	80	0.63
Er24	50	80	0.63
Er28	200	150	0.37

NB: $R_H = pH_2/(pH_2+pAr)$ is the hydrogen fraction.

3. Results and discussion

3.1 Structural and chemical characterisation

Fig. 1 shows the XRD and Raman spectra for the samples studied. All samples show the broad band related to the silicon amorphous matrix. The sample Er28 grown at higher RF power but in Ar rich atmosphere does not show any crystalline peak in both the XRD and Raman spectra. In contrast, the (111), (220) and (311) diffraction peaks of c-Si are visible for all the others samples. The peaks are well evident for the Er22 sample grown at high H2 dilution and at the high temperature of 400 ºC. The diffraction peaks have a lower intensity for the Er19 and Er24 samples, indicating a decrease of the crystallinity and/or grain size as also confirmed in the Raman spectra (Fig. 1b). The average crystal size presented in Table 2 was obtained by the fitting of the (111) c-Si diffraction peak [9]. To analyse the Raman spectra, we used a Gaussian profile for the amorphous TO structure and the crystalline

profile was calculated on the basis of Strong Phonon Confinement model [12]. Data in Tables 1 and 2 show that, for samples grown in H_2 rich atmosphere, both the average crystal size and the crystalline volume fraction increase with the substrate temperature. XRD and Raman spectroscopy yield average values of both crystalline fraction and crystallite size. More deep insight into the films structure can be obtained by SE. The best-fit BEMA models from which the structure is derived show a very complex layered structure due to the oxygen in-diffusion profile [13].
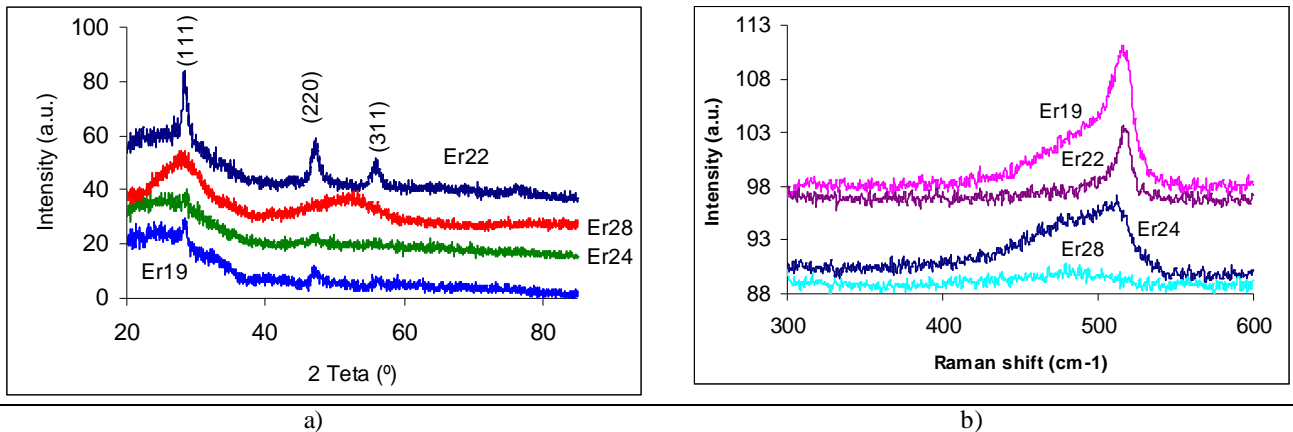

Figure 1: (a) XRD and (b) Raman spectra of the examined samples with different crystallinity.

Different pseudodielectric response points to the difference in microstructure of the samples studied. In particular, the Er22 sample shows pronounced E_1 and E_2 critical points in SE spectra that are distinctive interband transitions of c-Si. In contrast, the SE spectra of the Er19 and Er24 samples are characterized by low values of $<\varepsilon_2>$ and an extended interference pattern spreading to about 3 eV that provides an evidence for material large band-gap. These characteristics are indicative of a large volume fraction of the SiO phase (consistent with RBS) in films. Nevertheless, the presence of E_1 and E_2 inflection points is clearly seen in the second derivative of spectra, shown in Fig. 2, hence, confirming the involvement of crystallites in the films structure. The Er28 sample shows the $<\varepsilon_2>$ spectra with a single peak at about 3.6 eV representative for a-Si:H. Nevertheless, it has been found that the good fit of SE spectrum of this sample cannot be achieved by including only standard dielectric functions of hydrogenated a-Si and of SiO (see also the very small O% detected by RBS). The best-fit of SE spectrum was obtained by including a small volume fraction (25%) of small nc-Si (1–3 nm) embedded in a-Si:H tissue. Since this sample has very low oxygen content and large amount of hydrogen determined by RBS, the nanocrystallites should be mainly passivated by hydrogen.

Table 2
Atomic concentration and structural parameters

Sample	Er (%)	Si (%)	O (%)	H (%)	D_X (nm)	D_R (nm)	C_R (%)
Er22	0.10	71.7	8.8	17.6	7.0	7.9	65
Er19	0.12	62.0	34.0	23.0	5.7	6.5	43
Er24	0.17	56.5	17.6	25.4	3.9	5.5	23
Er28	0.11	60.9	2.9	34.3	–	–	0

D : average crystal size (R: Raman, X: X-ray); C_R : crystalline volume fraction by Raman.
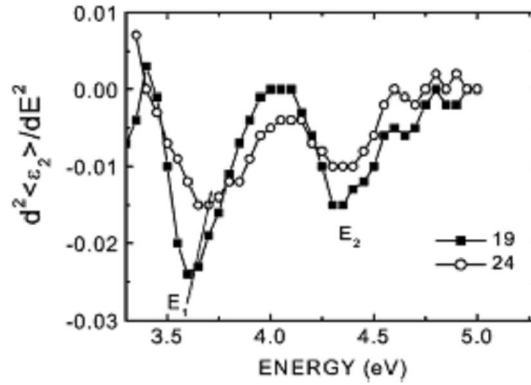
Figure 2: Second derivative spectra of the imaginary part of the pseudodielectric function, $d^2\langle\varepsilon_2\rangle/dE^2$, obtained for sample Er19 and Er24

3.2 Ellipsometry characterization

Fig. 3a shows the IR PL spectra at 77 K for the samples studied. All spectra are characterised by the presence of 1.537–1.539 mm peaks originated by interatomic $^4I_{13/2} \rightarrow {}^4I_{15/2}$ transitions of rare earth Er ions. In addition, with the increasing crystalline fraction in the samples, the lines at 1.06, 1.1, 1.4 and 1.34 μm (Fig. 3b) become pronounced in PL spectra indicating for the increasing role of silicon crystallites in PL response. In analogy with the crystalline silicon, the lines at 1.1, 1.06 and 1.4, 1.34 μm (Fig. 3b) could be assigned as the exciton- (1.1 and 1.06 μm) and dislocation- (1.4 and 1.34 μm) related PL bands appearing in the large diameter crystallites. Noteworthy, that we also observed the fine line pattern of 4f Er transitions (the lines at 1.537, 1.545, 1.55 μm in the inset of Fig. 3b) giving a direct evidence for the crystalline environment of Er ions and therefore, their location inside the Si nanocrystals in films.

Regarding the PL intensity, although the samples have a similar atomic percentage of Er impurity (0.1–0.17% as estimated by RBS), a drastic quenching of the intra-ionic PL was observed with the increase of the crystalline fraction and crystallite sizes. It seems that this decrease of PL is a consequence of the reduced excitation efficiency of Er ions and of the increasing role of non-radiative losses in the samples with the extended crystallinity. For the highly crystalline samples, one can imagine that the close neighbouring of Si crystallites will increase the propagation probability of the generated exitons in between the crystallites therefore, increasing the probability for alternative non-radiative recombination processes (for example the recombination on the crystallite grain boundaries). On the other hand, the lowering of the site symmetry for Er centres in amorphous as compared to the crystalline Si should also influence the luminescence efficiency; in particular the increase of the probability for the normally forbidden intra-4f transition of Er^{3+} ions should be expected. According to the analysis made in Ref. [14], the three-fold Er coordination in a-Si:H has a lower symmetry than the sixfold coordination found for Er in crystalline Si [15]. Thus, the basically amorphous nature of the Er28 sample can partially explain its maximal Er^{3+} PL intensity and the tendency for a decreasing of the Er-related PL in films with the stretching of the crystalline fraction. High Er^{3+} luminescence at room temperature was observed mainly in low crystalline and amorphous samples. So, for the sample Er28, the PL quenched only in about three times from 77 to 300 K.
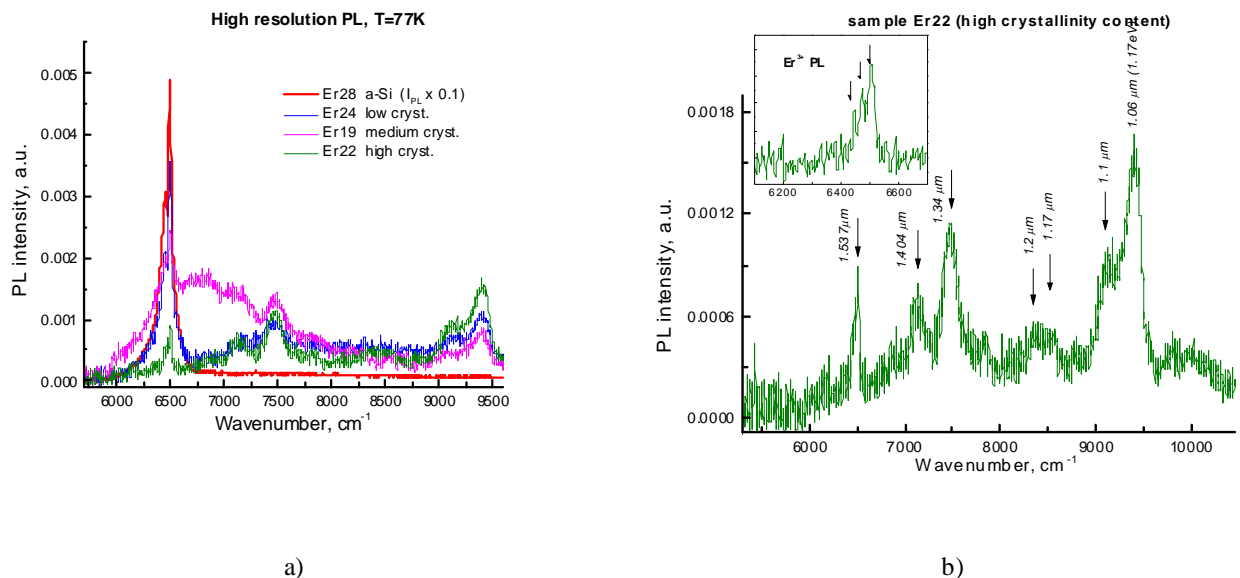
Fig. 3. IR PL spectra at 77 K obtained under 514.5 nm laser line excitation.(a) Comparison of the PL spectra for different samples studied: (red) Er28 (multiplied by 0.1); (blue) Er24; (pink) Er19; and (green), Er22 sample. (b) PL spectra of the high crystalline sample (Er22). Inset shows the enlarged spectrum for $^4I_{13/2} \rightarrow {}^4I_{15/2}$ transitions identified in the sample Er22.

4. Conclusions

In this work, we have discussed the structure, anatomy and IR PL properties of Er-doped nc-Si thin films prepared by RF co-sputtering. We have pointed out the correlation between the structure and PL response as a function of co-doping (with O, H), of crystallite sizes and as a function of crystal distributions (isolated or agglomerated) in the matrix. Efficient PL was observed in these structures at the wavelength of 1.54 μm without any high temperature post-growth annealing. nc-Si films, in which the nanocrystals with a size distribution in the range of 1–3 nm are embedded in an a-Si:H tissue show efficient Er^{3+} luminescence at 1.54 μm also at room temperature. They are characterized by a reduced luminescence thermal quenching.

References
[1] S. Coffa, L. Tsybeskov (Eds.), Silicon-based Optoelectronics, MRS Bulletin, vol. 23, 1998, p. 16.
[2] Y. Kanzawa, T. Kakeuka, M. Fujii, S. Hayashi, K. Yamamoto, Solid State Commun. 102 (1997) 533.
[3] M. Fujii, M. Yoshida, Y. Kanzawa, S. Hayashi, K. Yamamoto, Appl. Phys. Lett. 71 (1997) 1198.
[4] M. Fujii, M. Yoshida, S. Hayashi, K. Yamamoto, J. Appl. Phys. 84 (1998) 1.
[5] G. Qin, G.G. Qin, S.H. Wanget, J. Appl. Phys. 85 (1999) 6738.
[6] F. Priolo, G. Franzo, F. Lacona, D. Pacifici, V. Vinciguerra, Mater. Sci. Engng B 81 (2001) 9.
[7] P.G. Kik, A. Polman, Mater. Sci. Engng B 81 (2001) 3.
[8] M.F. Cerqueira, J.A. Ferreira, G.J. Adriaenssens, Thin Solid Films 370 (2000) 128.
[9] M.F. Cerqueira, M. Andritschky, L. Rebouta, J.A. Ferreira, M.F. da Silva, Vacuum 46 (1995) 1385.

[10] C. Summonte, R. Rizzoli, A. Desawo, F. Zignani, E. Centurioni, R. Pinghini, et al., Philos. Mag. B 80 (2000) 459.

[11] D.A.G. Bruggemann, Ann. Phys. (Leipzig) 24 (1965) 636.

[12] I.H. Campbell, P.M. Fauchet, Solid State Commun. 58 (1986) 739.

[13] M. Losurdo, M.F. Cerqueira, E. Alves, M.V. Stepikhova, M.M. Gangregon, G. Bruno, Phisica E (2003) in press.

[14] C. Piamonteze, A.C. Inigvez, L.R. Martins Alves, M. Tolentino, Phys. Rev. Lett. 81 (1998) 4652.

[15] D.L. Adler, D.C. Jacobson, D.J. Eaglesham, M.A. Marcus, J.C. Benton, J.M. Poate, et al., Appl. Phys. Lett. 61 (1992) 2128.